ACS Photonics

Article

Cite This: ACS Photonics 2019, 6, 2450−2454

pubs.acs.org/journal/apchd5

Plasmon-Polariton from a Helical State in a Dirac Magnet

Ivan Iorsh,*[,†] Gulnaz Rahmanova,[†] and Mikhail Titov[‡,†]

[†]ITMO University, Saint Petersburg 197101, Russia

[‡]Institute for Molecules and Materials, Radboud University, NL-6525 AJ Nijmegen, The Netherlands

ABSTRACT: Electromagnetic field interacting with a topologically protected one-dimensional electron helical state is shown to support a one-dimensional plasmon-polariton, which is a collective electron excitation dressed with the electromagnetic field. The electronic helical state arises at the surface of three-dimensional topological insulator in the proximity of the ferromagnet and is localized at the magnetization domain wall. This opens the possibilities to manipulate quantum optical states by altering magnetic domain configurations. An exact spectral equation for such topological plasmon-polariton is derived.

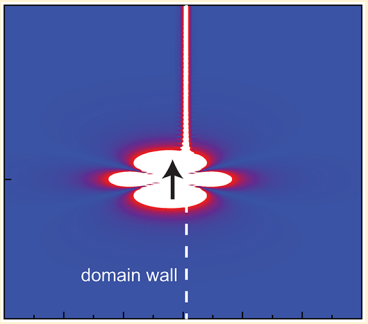

KEYWORDS: *Plasmon-Polariton, S-SNOM, Dirac semimetal*

The Dirac magnet is a model system that can be realized, e.g., in the form of a ferromagnet thin film in a close proximity to a surface of a three-dimensional (3D) topological insulator or topological semimetal. A perpendicular-to-the-plane magnetization component in the ferromagnet induces a finite effective mass of Dirac electrons in the topological insulator. As a result, such a magnetic proximity opens up a band gap in the Dirac electron spectrum, which destroys the two-dimensional (2D) Dirac surface state. However, a one-dimensional (1D) domain wall in the ferromagnet is imaged in the Dirac electron system as a zero mass line that supports a helical electronic state. The properties of such a state are similar to those of a quantum Hall edge state. The difference is that the helical state at the domain wall originates in the anomalous Hall effect in the Dirac magnet.

The physics proposed can be realized, e.g., in the Bi_2Se_3/EuS interface, where the magnetic proximity effect on topological states has been already experimentally demonstrated.[1,2] One can also expect similar phenomena in ZrSiS thin crystal[3] that is weakly coupled through an oxide layer to a ferromagnetic thin film.

In this Article, we investigate how these helical electronic states may give rise to 1D plasmon-polariton excitations in the presence of THz radiation. Excitation and detection of the plasmon-polaritons are illustrated in Figure 1 in a setup that is similar to the one used recently in a series of experiments with the scattering SNOM technique.[4,5]

For a sake of qualitative analysis, we choose the simplest model of the Dirac magnet that gives rise to helical electronic states, described by the Hamiltonian $\mathcal{H}$:[6]

$$\mathcal{H} = v\left[\boldsymbol{\sigma} \times \left(\boldsymbol{p} - \frac{e\boldsymbol{A}}{c}\right)\right]_z + \boldsymbol{\sigma}\cdot\boldsymbol{M}(\boldsymbol{r}) \tag{1}$$

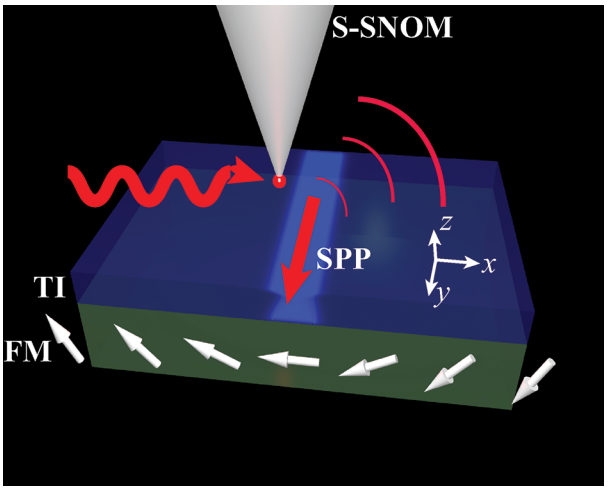

Figure 1. Schematic image of the near-field optical imaging of the ferromagnetic wall via the excitation of the plasmon-polariton in Dirac magnet. The profile of magnetization forming the domain wall is shown with white arrows.

where the direction $\hat{\boldsymbol{z}}$ is chosen perpendicular to the 2D surface, v is the effective velocity of Dirac quasiparticles ($v \approx 5 \times 10^5$ m/s), $\boldsymbol{p}$ is the momentum operator, $\boldsymbol{A}$ is the vector potential, e is the electron charge ($e = -|e|$), $i\boldsymbol{\sigma}$ is the 3D vector of Pauli matrices, and the classical vector field $\boldsymbol{M}(\boldsymbol{r})$ describes the proximity effect to a ferromagnet. The amplitude of the vector $|\boldsymbol{M}| = \Delta$ sets the strength of the exchange coupling between conduction electrons and localized momenta in the ferromagnet.

Received: May 10, 2019
Published: September 5, 2019

DOI: 10.1021/acsphotonics.9b00683
ACS Photonics 2019, 6, 2450−2454

We consider a flat domain wall that is elongated in the y-direction and has a characteristic width a_0 in the x-direction. We assume that, away from the domain wall, the magnetization is directed perpendicular to the electron plane $\boldsymbol{M} = -\Delta\hat{\boldsymbol{z}}$ for $x \ll -a_0$ and $\boldsymbol{M} = \Delta\hat{\boldsymbol{z}}$ for $x \gg a_0$. The value of exchange coupling $\Delta \approx 4$ meV defines the spectral gap in the electron spectrum (away from the domain wall). The corresponding length, $l_\Delta = \hbar v/\Delta \approx 80$ nm, sets the characteristic size of a localized electron wave function of the helical state in the x-direction. The domain wall is assumed to be smooth on atomic scales but sufficiently sharp on the scale of l_Δ, such that $a_0 \ll l_\Delta$. To avoid optical excitations of bulk states, one must further ensure that the frequency of electromagnetic radiation is smaller than the gap, $\omega \ll \Delta/\hbar \approx 1$ THz.

It is evident from eq 1 that the terms proportional to M_x and M_y components can be added to the vector potential. Those correspond to additional weak magnetic field in the vicinity of the domain wall that can be neglected. In what follows, we simply choose a particular model with $M_x = M_y = 0$ and $M_z(x) = \Delta\tanh(x/a_0)$. In the absence of electromagnetic radiation, this model gives rise to an exactly solvable spectral problem,

$$v[\boldsymbol{\sigma}\times\boldsymbol{p}]_z\Psi + \Delta\tanh\left(\frac{x}{a_0}\right)\sigma_z\Psi = \varepsilon\Psi \tag{2}$$

The solution of eq 2 for $|\varepsilon| < \Delta$ is given by a single helical state,

$$\Psi_k(\boldsymbol{r}) = \frac{1}{\sqrt{2}}\begin{pmatrix}1\\1\end{pmatrix}F_\nu(x)\phi_k(y) \tag{3}$$

with linear dispersion $\varepsilon_k = \hbar v k$. Here, $\phi_k(y)$ is a plane wave in the y-direction and $F_\nu(x)$ is a bounded wave function describing the profile of the helical state in the x-direction,

$$\phi_k(y) = \frac{1}{\sqrt{2\pi}}e^{iky}, \qquad F_\nu(x) = \frac{[a_0 B(1/2,\nu)]^{-1/2}}{\cosh^\nu(x/a_0)} \tag{4}$$

where the parameter $\nu = a_0/l_\Delta$ defines the wave function decay, while $B(1/2,\nu) = \Gamma(1/2)\Gamma(\nu)/\Gamma(1/2+\nu)$, entering the normalization factor, is the Euler beta function.

The state Ψ_k is evidently an eigenstate of the current operator $\hat{j}_y = ev\sigma_x$ that corresponds to the unidirectional current in the y-direction (the helical state with the opposite helicity would require M_z changing from positive to negative with increasing x).

In the limit $a_0 \ll l_\Delta$, one finds a particularly simple expression for the helical state profile: $F_0(x) = \exp(-|x|/l_\Delta)/\sqrt{l_\Delta}$.

The linear response of the current density $\boldsymbol{j}$ to the electric field $\boldsymbol{E}$ is defined in the frequency domain by

$$\boldsymbol{j}(\boldsymbol{r},\omega) = \int d^3\boldsymbol{r}'\hat{\sigma}(\boldsymbol{r},\boldsymbol{r}';\omega)\boldsymbol{E}(\boldsymbol{r}',\omega) \tag{5}$$

where $\hat{\sigma}(\boldsymbol{r},\boldsymbol{r}';\omega)$ is the conductivity tensor. Because of translational invariance in the y-direction, the corresponding Fourier transform can be taken in order to express the conductivity tensor in the mixed representation $\hat{\sigma}(x,z;x',z';q;\omega)$, where q is the wave vector in the y-direction.

We shall further assume that the chemical potential of electrons is well within the magnetization-induced gap, such that $|\mu \pm \hbar\omega| \ll \Delta$; hence, the THz radiation with frequency ω cannot excite electron states in the bulk. In this regime, the optical conductivity can be expressed by Kubo formula[7] that takes into account only the helical electron state, while the only nonvanishing component of the conductivity tensor is given by

$$\sigma_{yy}(x,z;x',z';q;\omega) = \frac{ie^2}{\hbar}v\delta(z)\delta(z')\frac{F_\nu^2(x)F_\nu^2(x')}{q(\omega - vq)} \times \int_{-\infty}^{\infty}\frac{dk}{2\pi}[f(\varepsilon_{k-q/2}) - f(\varepsilon_{k+q/2})] \tag{6}$$

where $f(\varepsilon) = [e^{(\varepsilon_k-\mu)/T} + 1]^{-1}$ is the Fermi distribution function. For $T \ll \Delta$, the integration in eq 6 is readily performed with the result

$$\sigma_{yy} = \bar{\sigma}_{\omega,q}F_\nu^2(x)F_\nu^2(x')\delta(z)\delta(z') \tag{7}$$

where we have defined a "one-dimensional" conductivity,

$$\bar{\sigma}_{\omega,q} = -\frac{1}{2\pi i}\left(\frac{\alpha v}{k_0 - qv/c}\right) \qquad k_0 = \omega/c \tag{8}$$

with $\alpha = e^2/\hbar c \approx 1/137$, standing for the fine structure constant.

The result of eq 8 describes a 1D plasmon with the trivial linear dispersion $\omega_q = vq$. It is known in the theory of 1D electronic systems[8−10] that, in contrast to single electron excitations, such a plasmon may remain a good quasi-particle, even in the presence of interactions. Moreover, it has been shown that the analogous quasi-1D plasmons arising in various 2D electron systems subject to spatially inhomogeneous potentials are characterized by extremely long lifetimes, compared to their 2D counterparts.[11,12]

In our problem, the quasi-1D plasmon mode originates from the quantized 1D electron helical state. However, the 1D plasmons may also emerge from the bulk 2D continuum in the case of the spatially modulated conductivity.[13]

When THz radiation is applied to the system, as shown in Figure 1, the plasmon is transformed to another quasiparticle that is called plasmon-polariton. To find its dispersion, it is necessary to solve the Maxwell equation,

$$\text{rot rot}\,\boldsymbol{E}(\boldsymbol{r},\omega) = k_0^2\boldsymbol{E}(\boldsymbol{r},\omega) - \frac{4i\pi k_0}{c}\boldsymbol{j}(\boldsymbol{r},\omega) \tag{9}$$

with the electric current $\boldsymbol{j}$ defined by eq 5. This equation is equivalent to the integral equation of the form,

$$E_\gamma(\boldsymbol{r},\omega) = i\frac{4\pi k_0}{c}\sum_{\alpha\beta}\int d^3\boldsymbol{r}'G_{\gamma\alpha}(\boldsymbol{r}-\boldsymbol{r}';\omega) \times \int d^3\boldsymbol{r}''\sigma_{\alpha\beta}(\boldsymbol{r}',\boldsymbol{r}'';\omega)E_\beta(\boldsymbol{r}'',\omega) \tag{10}$$

where $G_{\alpha\beta}(\boldsymbol{r}-\boldsymbol{r}';\omega)$ represents the dyadic Green's function in a vacuum.

Equation 10 is nontrivial only for the component E_y. Taking into account again the translational invariance in y direction, we obtain

$$E_y(x,z;q;\omega) = i\bar{\sigma}_{\omega,q}\frac{4\pi k_0}{c}\int dx'G_{yy}(x-x',z;q) \times F_\nu^2(x')\int dx''F_\nu^2(x'')E_y(x'',0;q;\omega) \tag{11}$$

where we introduce the Fourier-transformed Green's function $G_{yy}(x-x',z-z';q)$ in the mixed representation.

DOI: 10.1021/acsphotonics.9b00683
ACS Photonics 2019, 6, 2450−2454

To obtain the spectral equation on plasmon-polariton, we multiply eq 11 by $F_\nu^2(x)\delta(z)$ and integrate over x and z. The procedure leads to the relation

$$1 = i\bar{\sigma}_{\omega,q}\left(\frac{4\pi k_0}{c}\right)\int\int \mathrm{d}x\ \mathrm{d}x' F_\nu^2(x) G_{yy}(x-x') F_\nu^2(x') \tag{12}$$

where $G_{yy}(x-x') = G_{yy}(x-x', 0; q)$. This Green's function can be represented as

$$G_{yy}(x-x') = \frac{1}{2k_0^2}\int \frac{\mathrm{d}k}{2\pi}\frac{k_0^2 - q^2}{\sqrt{k^2+q^2-k_0^2}} e^{ik(x-x')} \tag{13}$$

Substituting eq 13 in eq 12, we perform the integrations over x and x' analytically with the result

$$1 = \frac{i\bar{\sigma}_{\omega,q}}{\omega}\frac{k_0^2 - q^2}{\Gamma^4(\nu)}\int_{-\infty}^{\infty}\mathrm{d}u \frac{|\Gamma(\nu(1+iu/2))|^4}{\sqrt{u^2 - l_\Delta^2(k_0^2 - q^2)}} \tag{14}$$

that defines the exact dispersion relation ω_q for the surface plasmon-polariton.

It is instructive to analyze the dispersion relation defined by eq 14 in the limit $\nu = a_0/l_\Delta \ll 1$. For $\nu = 0$, eq 14 is simplified to

$$1 - \tilde{v}\tilde{q} = \alpha\tilde{v}(\tilde{q}^2 - 1)\mathcal{S}(\kappa)/2\pi \tag{15}$$

where $\tilde{q} = qc/\omega$, $\tilde{v} = v/c$, $\kappa^2 = 1 + l_\Delta^2(k_0^2 - q^2)/4$, and

$$\mathcal{S}(\kappa) = \int_{-\infty}^{\infty}\mathrm{d}u(1+u^2)^{-2}(1+u^2-\kappa^2)^{-1/2} = \kappa^{-3}[(1+\kappa^2)\mathrm{arctanh}(\kappa) - \kappa] \tag{16}$$

Furthermore, we note that the condition $\hbar\omega \ll \Delta c/v$ is always fulfilled; consequently, $l_\Delta k_0 \ll 1$. Thus, for sufficiently small momenta ($q \ll l_\Delta^{-1}$), we can always regard the parameter $1 - \kappa^2$ as small and positive. In this limit, we can simply rewrite eq 15 as

$$1 - \tilde{v}\tilde{q} = \frac{\alpha}{2\pi}\tilde{v}(\tilde{q}^2 - 1)\left[\ln\left(\frac{16}{l_\Delta^2(q^2 - k_0^2)}\right) - 1\right] \tag{17}$$

This equation can be explicitly solved in the limit $\omega \ll qc$ (or $\tilde{q} \gg 1$) with the result

$$\omega_q^{\pm} = \frac{qv}{2}\left\{1 \pm \sqrt{1 + \frac{2\alpha c}{\pi v}\left[\ln\left(\frac{16}{q^2 l_\Delta^2}\right) - 1\right]}\right\} \tag{18}$$

Note that we formally restore the plasmon dispersion for $\alpha = 0$. Taking the leading logarithm approximation in eq 18, we obtain a particularly simple relation

$$\omega_q^{\pm} = \pm qv\sqrt{\frac{\alpha c}{\pi v}\ln\left(\frac{1}{|q|l_\Delta}\right)} \qquad q \ll \frac{1}{l_\Delta} \tag{19}$$

where the branches ω^+ and ω^- correspond to positive and negative values of the momentum q, respectively. However, the symmetry between the branches is broken for q approaching $1/l_\Delta$. To describe the dispersion relation at sufficiently large values of momenta, one still must refer to eq 14 or eq 15.

In Figure 2, we illustrate the dispersion relation obtained numerically from eqs 14 and 15 for realistic parameter values. We find that, for $q > 1/l_\Delta$, the dispersion differs substantially from the one for the Hall effect edge magneto-plasmon polariton.[14]

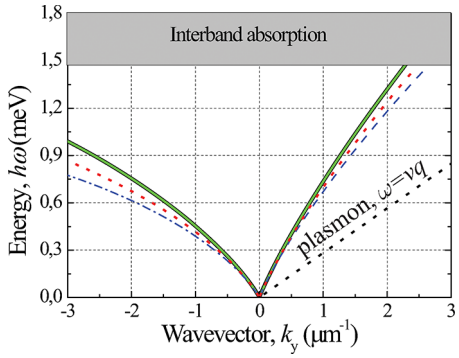

Figure 2. Dispersion of the one-dimensional (1D) topological plasmon polariton for characteristic material parameters of FM/ZrSiS heterostructure, where q is the wave vector component along the electron helical state. For $q \ll 1/l_\Delta \approx 5\ \mu\mathrm{m}^{-1}$, the two branches of the dispersion are almost symmetric and are given by eq 19. For $q \gtrsim 1/l_\Delta$, one observes strong asymmetry of the branches. Different lines correspond to different choices of the domain wall width $a_0 = \nu l_\Delta$: black line ($\nu = 0$), green line ($\nu = 0.05$), dotted red ($\nu = 1$), and dashed blue ($\nu = 2$). Other parameters of the calculation are listed in the text.

For realistic analysis, one still must take into account the presence of the substrate by replacing the dyadic Green's function in eq 12 with the one for a particular heterostructure. The latter can be routinely calculated for an arbitrary layered system.[15] Here, we still refer to eqs 14 and 15 with the parameters that are characteristic for a surface of ZrSiS[3] in proximity to a generic ferromagnetic film with a saturation magnetization of 0.5 T. In such a setup, we have $\Delta \approx 1.5$ meV and $v \approx 4.3 \times 10^5$ m/s, consequently, we find $l_\Delta \approx 0.2\ \mu$m.

In Figure 2, we plot the dispersion of the plasmon polariton defined by eq 14 for different values of $a_0 = \nu l_\Delta$. A typical domain wall with a width of $a_0 \approx 10$ nm corresponds to $\nu \approx 0.05$. It can be seen that the dispersion for the case of $\nu = 0.05$ does agree very well with the one given by eq 15 for $\nu = 0$. The discrepancies between the results of eqs 14 and 15 become visible only for $\nu \approx 1$. For small values of momenta, the results are well-described by the limiting expression of eq 19. We note that our choice of parameters correspond to $\alpha c/\pi v \approx 1.6$.

In the case of finite temperatures, the interband absorption should be taken into consideration. This would result in the nonzero real part of the dynamical conductivity. The expression for $\tilde{\sigma}_{\omega,q}$ then yields

$$\tilde{\sigma}_{\omega,q} = \frac{i}{2\pi}\left(\frac{\alpha v}{k_0 - qv/c + i\gamma}\right) \tag{20}$$

where γ stems for the interband absorption. This, in turn, would result in the finite propagation length of the plasmon-polariton. The propagation length l_{prop} at temperature T can be roughly estimated as

$$l_{\mathrm{prop}} \approx e^{(m-\hbar\omega)/kT} q_y^{-1} \tag{21}$$

At $T = 1$ K and at the polariton frequency $\omega = \Delta/2 = 0.75$ meV, the propagation length is 1.8 mm for the right-propagating polariton and 0.9 mm for the left propagating polariton.

DOI: 10.1021/acsphotonics.9b00683
ACS Photonics 2019, 6, 2450−2454

Let us now consider a particular scenario for the excitation of the helical plasmon-polariton. For that, we adopt the scattering SNOM technique, which has been used to visualize the propagation of the 2D and edge plasmons in several systems.[4,5,16] Within this approach, a tip of SNOM is located in the vicinity of the domain wall. A coherent electromagnetic signal then is focused by an antenna to the tip end. The tip then scatters the radiation as a point dipole. The near field of the scattered signal then excites the resonant plasmonic modes. The propagating plasmonic mode can then be scattered by the tip to the far field and be collected by the detector. This allows one to measure the real space intensity profile of the 2D and 1D plasmon polaritons. While conventionally, tips scatter as dipoles oriented perpendicular to the surface, the polarization can be controlled by engineering of the tip shape.[17] Here, for the sake of clarity, we consider the scattered field by a y-polarized point dipole located in a vicinity of the domain wall, $\boldsymbol{r}_0 = (x_0, 0, z_0)$. The y-component of the electric field is given by

$$E_y(x, z, q; \omega) = G_{yy}(x - x_0, z - z_0; q) + \alpha\tilde{v}\Lambda(q, x_0, z_0)\int \mathrm{d}x' G_{yy}(x - x', z; q)F_\nu^2(x') \quad (22)$$

where we again adopt the mixed representation of the dyadic Green's function used in eq 11, and

$$\Lambda(q, x_0, z_0) = \frac{\int \mathrm{d}x'' G_{yy}(x'' - x_0, -z_0; q)F_\nu^2(x'')}{1 - \tilde{v}\tilde{q} - \alpha\tilde{v}(\tilde{q}^2 - 1)\mathcal{S}(\kappa)/2\pi + i\gamma} \quad (23)$$

In Figure 3a, we plot the second term at the right-hand side of eq 22 that represents the Fourier transform of the y-component of the electric field scattered by the domain wall. In the plot, we choose $\hbar\omega = 0.75$ meV, $\boldsymbol{r}_0 = (-5, 0, 0.1)$ μm, and $\gamma = 0.002$.

The plot shows that, besides the broad distribution of the near field, there exist two narrow peaks corresponding to the excitation of the surface plasmon polaritons (marked with dashed white ellipses). Indeed, the central positions of these peaks match the dispersion relation of eqs 14,17 (see Figure 2) at the corresponding frequency.

Also note that both the peak positions and the peak intensity are somewhat different for positive and negative q (for $|q| \gtrsim 1/l_\Delta$) highlighting the helicity of the corresponding electron state. In Figure 3b, we show the real space map of the y-component of the electric field given by eq 22. The map illustrates the field scattered by the point dipole, which excites the domain wall plasmon-polariton. First of all, as can be seen, the excitation of the chiral plasmon polariton is asymmetric. This is due to the fact that, because of the finite absorption, the propagation lengths of the right and left moving plasmons are different. This can be seen in detail in Figure 3c, where the plot of $|E_y|$ at $x = 0$ is plotted. Moreover, the oscillations of the electric field modulus are observable. These oscillations arise due to the interference of the field directly scattered by the tip end and the plasmon polariton field. The period of the oscillations L is dependent on the wavevector of plasmon polariton as $(q_y - k_0)L = 2\pi$. For the right propagating plasmon polariton, the period is equal to 6.3 μm, which corresponds to $q_y \approx 1$ $\mu\mathrm{m}^{-1}$, coinciding with the analytical expression. The left propagating plasmon polariton decays rapidly; however, the oscillations are still present (see Figure 3d) and the period corresponds to $q_y \approx 2$ $\mu\mathrm{m}^{-1}$, which also coincides with the analytical result. Thus, the dispersion of the plasmon-polariton can be probed directly in the near-field scanning optical microscopy measurements.

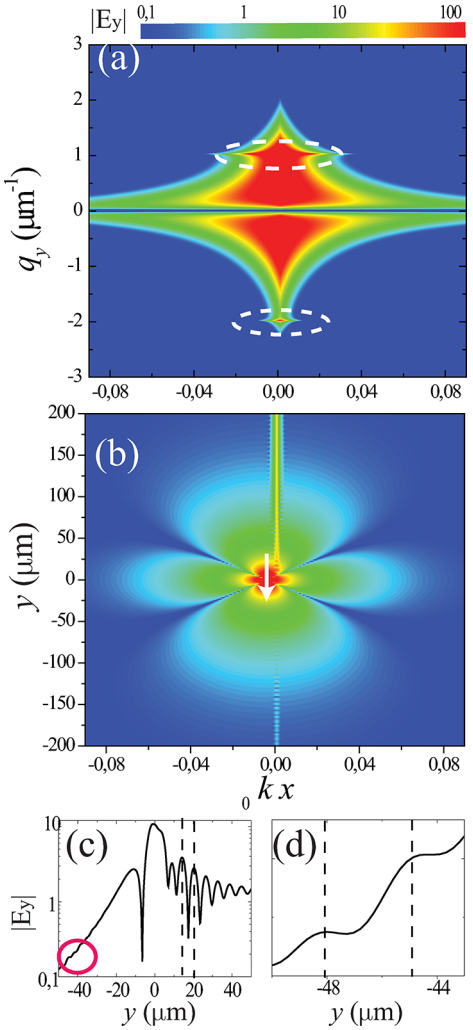

Figure 3. (a) Fourier map of the scattered electric field from a dipole positioned at $\boldsymbol{r}_0 = (-5, 0, 1)$ μm, assuming the dipole frequency $\hbar\omega = 0.75$ meV. The dashed regions show the excitation of the surface plasmon modes. (b) Real space map of the $|E_y|$. (c) E_y profile at $x = 0$. (d) Enlarged view of the region marked with a red ellipse in panel (c).

In conclusion, we considered a model of a helical electron state that can be formed along at a surface of 3D topological insulator or topological semi-metal that is brought into proximity to a ferromagnetic thin film with a flat domain wall. Such a state is analogous to the quantum Hall edge state but arises because of the anomalous Hall effect. We demonstrated that the state supports domain wall plasmon-polariton excitations and computed, for a simple model, the plasmon-polariton dispersion relation. We discuss a possibility to observe the effect with THz near-field scanning optical microscopy.

AUTHOR INFORMATION

Corresponding Author

*E-mail: i.iorsh@metalab.ifmo.ru.

ORCID

Ivan Iorsh: 0000-0003-4992-6122

DOI: 10.1021/acsphotonics.9b00683
ACS Photonics 2019, 6, 2450−2454

Notes

The authors declare no competing financial interest.

■ ACKNOWLEDGMENTS

M.T. acknowledges the support from the Russian Science Foundation, under Project 17-12-01359, and the support from the JTC-FLAGERA Project GRANSPORT. I.I. acknowledges the support of the Grants of the Ministry of Russian Federation (Nos. 3.1365.2017/4.6 and 14.Y26.31.0015), and the Grant of President of Russian Federation (No. MK-6248.2018.2).

■ REFERENCES

(1) Lee, A. T.; Han, M. J.; Park, K. Magnetic proximity effect and spin-orbital texture at the Bi_2Se_3/EuS interface. *Phys. Rev. B: Condens. Matter Mater. Phys.* **2014**, *90*, 155103−155111.

(2) Lee, C.; Katmis, F.; Jarillo-Herrero, P.; Moodera, J. S.; Gedik, N. Direct measurement of proximity-induced magnetism at the interface between a topological insulator and a ferromagnet. *Nat. Commun.* **2016**, *7*, 12014−12019.

(3) Hu, J.; Tang, Z.; Liu, J.; Zhu, Y.; Wei, J.; Mao, Z. Nearly massless Dirac fermions and strong Zeeman splitting in the nodal-line semimetal ZrSiS probed by de Haas−van Alphen quantum oscillations. *Phys. Rev. B: Condens. Matter Mater. Phys.* **2017**, *96*, 045127−045139.

(4) Chen, J.; Badioli, P.; Alonso-González, S.; Thongrattanasiri, F.; Huth, J.; Osmond, M.; Spasenović, A.; Centeno, A.; Pesquera, P.; Godignon.; et al. Optical nano-imaging of gate-tunable graphene plasmons. *Nature* **2012**, *487*, 77−81.

(5) Fei, Z.; Rodin, A. S.; Andreev, G. O.; Bao, W.; McLeod, A. S.; Wagner, M.; Zhang, L. M.; Zhao, Z.; Thiemens, M.; Dominguez, G.; et al. Gate-tuning of graphene plasmons revealed by infrared nano-imaging. *Nature* **2012**, *487*, 82−85.

(6) Qi, X.-L.; Zhang, S.-C. Topological insulators and superconductors. *Rev. Mod. Phys.* **2011**, *83*, 1057−1110.

(7) Haug, H.; Koch, S. W. *Quantum Theory of the Optical and Electronic Properties of Semiconductors*, Fifth Edition; World Scientific Publishing Company, 2009.

(8) Carmelo, J. M. P.; Castro Neto, A. H. Electrons, pseudoparticles, and quasiparticles in the one-dimensional many-electron problem. *Phys. Rev. B: Condens. Matter Mater. Phys.* **1996**, *54*, 11230−11244.

(9) Ng, T.-K. Functional Integral approach to quasi-particles in Fermi liquid theory. *arXiv Preprints*, arXiv preprint cond-mat/9706033, 1997.

(10) Castellani, C.; Di Castro, C. Breakdown of Fermi Liquid in correlated electron systems. *Phys. A* **1999**, *263*, 197−207.

(11) Hasdeo, E.; Song, J. Long-Lived Domain Wall Plasmons in Gapped Bilayer Graphene. *Nano Lett.* **2017**, *17*, 7252−7257.

(12) Song, J.; Rudner, M. Chiral plasmons without magnetic field. *Proc. Natl. Acad. Sci. U. S. A.* **2016**, *113*, 4658−4663.

(13) Smith, T. B.; Torre, I.; Principi, A. Edge modes and Fabry-Perot plasmonic resonances in anomalous-Hall thin films. *Phys. Rev. B: Condens. Matter Mater. Phys.* **2019**, *99*, 155422−155431.

(14) Volkov, V.; Mikhailov, S. A. Edge magnetoplasmons: low frequency weakly damped excitations in inhomogeneous two-dimensional electron systems. *Sov. Phys. JETP* **1988**, *67*, 1639−1653.

(15) Tomaš, M.-S. Green function for multilayers: Light scattering in planar cavities. *Phys. Rev. A: At., Mol., Opt. Phys.* **1995**, *51*, 2545.

(16) Alonso-González, P.; Nikitin, A. Y.; Golmar, F.; Centeno, A.; Pesquera, A.; Vélez, S.; Chen, J.; Navickaite, G.; Koppens, F.; Zurutuza, A.; Casanova, F.; Hueso, L. E.; Hillenbrand, R. Controlling graphene plasmons with resonant metal antennas and spatial conductivity patterns. *Science* **2014**, *344*, 1369−1373.

(17) Kim, D.-S.; Kim, Z. H. Role of in-plane polarizability of the tip in scattering near-field microscopy of a plasmonic nanoparticle. *Opt. Express* **2012**, *20*, 8689−8699.

DOI: 10.1021/acsphotonics.9b00683
ACS Photonics 2019, 6, 2450−2454